Materials Research Bulletin 140 (2021) 111314

Contents lists available at ScienceDirect

Materials Research Bulletin

journal homepage: www.elsevier.com/locate/matresbu

Synthesis, structure, melting and optical properties of three complex orthorhombic sulfides $BaDyCuS_3$, $BaHoCuS_3$ and $BaYbCuS_3$

Nikita O. Azarapin [a], Victor V. Atuchin [b,c,*], Nikolai G. Maximov [d], Aleksandr S. Aleksandrovsky [e,f], Maxim S. Molokeev [g,h,i], Aleksandr S. Oreshonkov [h,j], Nikolai P. Shestakov [j], Alexander S. Krylov [j], Tatyana M. Burkhanova [a], Shaibal Mukherjee [k], Oleg V. Andreev [a,l]

[a] Institute of Chemistry, Tyumen State University, Tyumen, 625003, Russia
[b] Laboratory of Optical Materials and Structures, Institute of Semiconductor Physics, SB RAS, Novosibirsk, 630090, Russia
[c] Research and Development Department, Kemerovo State University, Kemerovo, 650000, Russia
[d] Institute of Chemistry and Chemical Technology, Federal Research Center KSC SB RAS, Krasnoyarsk, 660049, Russia
[e] Laboratory of Coherent Optics, Kirensky Institute of Physics Federal Research Center KSC SB RAS, Krasnoyarsk, 660036, Russia
[f] Institute of Nanotechnology, Spectroscopy and Quantum Chemistry, Siberian Federal University, Krasnoyarsk, 660041, Russia
[g] Laboratory of Crystal Physics, Kirensky Institute of Physics, Federal Research Center KSC SB RAS, Krasnoyarsk, 660036, Russia
[h] Siberian Federal University, Krasnoyarsk, 660041, Russia
[i] Department of Physics, Far Eastern State Transport University, Khabarovsk, 680021, Russia
[j] Laboratory of Molecular Spectroscopy, Kirensky Institute of Physics Federal Research Center KSC SB RAS, Krasnoyarsk, 660036, Russia
[k] Hybrid Nanodevice Research Group (HNRG), Electrical Engineering and Centre for Advanced Electronics (CAE), Indian Institute of Technology Indore, Madhya Pradesh, 453552, India
[l] Laboratory of the Chemistry of Rare Earth Compounds, Institute of Solid State Chemistry, UB RAS, 620137, Ekaterinburg, Russia

ARTICLE INFO

Keywords:
Complex sulfides
Crystal structure
SEM
Raman
Melting point

ABSTRACT

Complex sulfides $BaDyCuS_3$, $BaHoCuS_3$ and $BaYbCuS_3$ were synthesized in a flow of sulfiding gases (CS_2, H_2S) at 900°C from standard solutions of lanthanide and copper nitrates, as well as from the same standard $Ba(OH)_2$ solution. The crystal structures of $BaDyCuS_3$, $BaHoCuS_3$ and $BaYbCuS_3$ were obtained by the Rietveld refinement method. All three compounds crystallize in the *Cmcm* space group ($KZrCuS_3$ structural type) as predicted by the tolerance factor analysis. Their micromorphological, thermal and spectroscopic properties are evaluated. $BaDyCuS_3$ and $BaHoCuS_3$ melt congruently at 1376.5 °C and 1363.8 °C. $BaYbCuS_3$ melts incongruently at 1353.3 °C. The optical band gap is 2.45 eV for $BaDyCuS_3$, 2.37 eV for $BaHoCuS_3$ and 1.82 eV for $BaYbCuS_3$. The low bandgap of $BaYbCuS_3$ is explained by the charge transfer band of Yb at the bottom of conduction band. The vibrational parameters of $BaDyCuS_3$, $BaHoCuS_3$ and $BaYbCuS_3$ crystals were determined with the use of Raman and Infrared spectroscopies.

1. Introduction

Many chalcogenide semiconductor crystals have interesting structural, chemical and physical properties, and such materials are in demand in the fields of electronics and optics [1–17]. The quaternary chalcogenide compounds containing transition and rare-earth elements are of particular interest because, in this case, wide freedom in the cation combination provides a possibility for the change of structure type and drastic variation of bandgap, electrical and optical characteristics. In this strategy, a lot of quaternary crystals, among sulfides and selenides, with valuable physical parameters were discovered [5,18–26]. Among the compounds, the chalcogenides with general composition $ABCX_3$ were considered, where A is an alkaline or alkaline earth (or analogs) metal, B is a d- or f-element, C is another d-element and X is a chalcogenide [1]. It was established that this type of compounds can crystallize in seven structural types: $KZrCuS_3$ (*Cmcm*), Eu_2CuS_3 (*Pnma*), Ba_2MnS_3 (*Pnma*), $BaCuLaS_3$ (*Pnma*), $BaAgErS_3$ (*C2/m*), $NaCuTiS_3$ (*Pnma*) and $TlCuTiTe_3$ ($P2_1/m$) [1]. In addition to the synthesis and crystal structures of these compounds, the semiconductor, magnetic, optical and thermodynamic properties were described for selected compositions [1,

* Corresponding author at: Institute of Semiconductor Physics, Novosibirsk, 630090, Russia.
E-mail address: atuchin@isp.nsc.ru (V.V. Atuchin).

https://doi.org/10.1016/j.materresbull.2021.111314
Received 7 December 2020; Received in revised form 9 March 2021; Accepted 11 March 2021
Available online 15 March 2021

15,17,27–34].

Recently, scrupulous investigations have been performed in the domain of plasmonic inclusion at the surface, bulk or thin film interface to increase the efficiency of chalcogenide semiconductor based solar cells [35]. The solar cell usually has a CdS buffer layer to prevent shunting, however there are certain issues with this buffer layer such as toxic Cd waste, absorb light with photon energy greater than ~2.38 eV etc. [36]. Moreover, advanced technologies in the form of multi-junction solar cell and multiple quantum well solar cell have got much attention, as these technologies have the ability to reduce the losses associated with the single junction solar cell incorporating chalcogenide materials [37,38]. The development of targeted electronic technologies offered the prospects for the application of Cu-containing sulfides and selenides in thin film structures, including solar cells and thermoelectric elements, because these chalcogenides are characterized by strong light absorptions over the visible spectral range and appropriate thermoelectric figure of merit [8,13,39–43]. Inspired by this activity, to extend the spectrum of available materials, the $ALnCuX_3$ compounds are of particular interest because Ln elements are of rich crystal chemistry and have specific spectroscopic properties. The known Ba-containing $BaLnCuS_3$ compounds crystallize in structural types of Eu_2CuS_3 (*Pnma*) or $KZrCuS_3$ (*Cmcm*) [1]. As it is known, both these structures are formed by the layers of CuS_4 tetrahedra and LnS_6 octahedra [44,45]. Previously, the structures were determined for $BaLnCuS_3$ (Ln = La, Pr (*Pnma*) and Ln = Sm, Er (*Cmcm*)) [18,27,46]. The unit cell parameters were also reported for $BaGdCuS_3$ [18]. The structural and physical properties of other compounds $BaLnCuS_3$ remain unclear.

The present work is aimed at the preparation of $BaLnCuS_3$ (Ln = Dy, Ho, Yb) compounds. These compounds were not synthesized earlier. However, according to the tolerance factor analysis implemented in [46], the crystallization is assumed in space group *Cmcm*. The quasi-ternary phase diagrams BaS -Ln_2S_3-Cu_2S for Ln = Dy, Ho, Yb were not investigated previously, but several similar systems for other rare earth metals were considered and the complex equilibrium patterns, involving peritectic/eutectic interactions and extensive ranges of solid solutions, were found [31,32,47–49]. As a consequence, the conditions of the synthesis of $BaDyCuS_3$, $BaHoCuS_3$ and $BaYbCuS_3$ may be not trivial. In the present experiment, $BaLnCuS_3$ (Ln = Dy, Ho, Yb) compounds are prepared by the sulfidation technique, and final powder products are studied in detail to see their structural, morphological and spectroscopic characteristics.

2. Experimental section

2.1. Synthesis

$BaDyCuS_3$, $BaHoCuS_3$ and $BaYbCuS_3$ compounds were prepared in powder forms by the sulphidation of oxide mixtures obtained after the decomposition of metal nitrate solutions. In the synthesis, the key steps were the same for all compounds. The high purity starting reagents were used: Cu (999 %, SZB Tsvetmet, Russia), $Ba(OH)_2$ the standard titrimetric substance (0.1 mol/L, LenReactive, Russia), Dy_2O_3 (99,99 %, ultrapure, TDM-96 Ltd. Russia), Ho_2O_3 (99,99 %, ultrapure, TDM-96 Ltd. Russia), Yb_2O_3 (99,99 %, ultrapure, TDM-96 Ltd. Russia) and concentrated nitric acid solution ($C(HNO_3)$ =14.6 mol/L, ultrapure, Vekton Ltd., Russia). Ammonium rodanide NH_4SCN (98 %, Vekton Ltd., Russia) was used as a source of sulfiding gases. Weighing them was carried out on the assay balances of Mettler Toledo at the accuracy of 0.1 mg. Before weighing, to remove the surface oxide, a ~1 mm in thick copper plate was etched in the $HClO_3$ solution and washed out in distilled water. Then, the Cu plate was cut into segments of ~1–5 mm^2. All starting metal oxides were calcinated in quartz crucibles at 1300 K for 5 h in the air to remove surface adsorbates and decompose the hydrocarbonates commonly present on the rare-earth oxide surface.

The $Ba(OH)_2$ solution was prepared from the standard titrimetric substance (0.1 mol/L, LenReactive, Russia). Dysprosium, holmium and ytterbium nitrates were prepared from the calcined rare-earth oxides. The weighed charge of Ln_2O_3 oxide was dissolved in ~ 20 mL of concentrated nitric acid. The solution was brought into a measuring flask and brought to the label with bidistillated water. A copper II nitrate solution was prepared from metallic copper by dissolving in ~ 20 mL of concentrated nitric acid followed by a transfer to a measuring flask. The solution was also brought to the label with bidistillated water. As a result, there is the following set of solutions with exact concentrations: $C(Ba(OH)_2) = 0.1$ mol/L, $C(Cu(NO_3)_2) = 1.0$ mol/L, $C(Dy(NO_3)_3) = 1.0$ mol/L, $C(Ho(NO_3)_2) = 1.0$ mol/L, $C(Yb(NO_3)_3) = 1.0$ mol/L. To prepare a nitrate mixture solution, 50 mL $Ba(OH)_2$, 5 mL $Ln(NO_3)_3$ and 5 mL $Cu(NO_3)_2$ were selected. All volumes were transferred to heat-resistant measuring glass.

The mixed solution was evaporated and the dry residue was decomposed at 900 °C. Then, the mixture was subjected to the thermal treatment in a flow of sulfiding gases [46]. At the end stage of reaction, the sulfiding gas stream was percolated, but the argon flow was left to remove excess sulfur and avoid a subsequent condensation of NH_4CSN decomposition products. The quartz reactor was removed from the furnace and cooled to room temperature without blocking the argon stream. The photo of obtained powder products of $BaDyCuS_3$ (yellow), $BaHoCuS_3$ (green-yellow) and $BaYbCuS_3$ (violet) are given in Fig. 1.

2.2. Characterization

The powder X-ray diffraction data of $BaLnCuS_3$ (Ln = Dy, Ho, Yb) for Rietveld analysis were collected at room temperature with a Bruker D8 ADVANCE powder diffractometer (Cu-Kα radiation) and linear VANTEC detector. The step size of 2θ was 0.016°, and the counting time was 6 s per step. All peaks were indexed by the orthorhombic cell (*Cmcm*) with parameters close to those of $BaNdCuS_3$ [18]. Therefore, this structure was taken as a starting model for the Rietveld refinement which was performed using package TOPAS 4.2 [50].

Fig. 1. Photo of (a) $BaDyCuS_3$, (b) $BaHoCuS_3$ and (c) $BaYbCuS_3$ products.

The particle micromorphology was observed by SEM using a JSM-6510LV-EDS device. For the SEM analysis, the powder sample was transferred onto an conductive carbon adhesive tape. The adhesive tape was attached to a copper cylinder with the diameter of 1 cm and the height of 1.5 cm. The sample was filled on top and the residues were shaken to avoid non-sticking particles.

The simultaneous thermal analysis was performed in the He (99999 %, Russia) flow with the use of a STA 449 F3 Jupiter instrument equipped with a (W3%Re – W25 %Re) thermocouple. The analyzed powder sample weight was (90–100)±0.01 mg. The temperature adjustment accuracy was not above 0.3 K. In the temperature range, where thermal events were observed, the heating rate was 20 K/min. The results of DSC/TG experiments were processed in the Proteus-6 software package [51]. The possible error in the phase transition enthalpy determination was 3 % and, for the melting temperature, it was 2−3 °C.

The Raman scattering spectra of $BaDyCuS_3$ and $BaYbCuS_3$ were collected in the backscattering geometry using a Horiba JobinYvon T64000 Raman spectrometer (Jobin Yvon, France). The spectral resolution for the recorded Raman spectra was about 1 cm^{-1} and a single-mode krypton laser Lexel Kr^+ (647.1 nm) was used as an excitation light source. The Raman scattering spectrum of $BaHoCuS_3$ was collected using a Bruker RFS100/S Raman spectrometer (Bruker, Germany). In this case, the 1064 nm Nd:YAG laser radiation was used as an excitation light source and the spectral resolution was about 1 cm^{-1}. A Fourier-transform spectrometer VERTEX 70 V (Bruker, Germany) was used to record the IR (Infrared) absorption spectra with spectral resolution 4 cm^{-1}. The spectrum was taken from the samples shaped as thick tablets prepared from the mixture of the investigated compound thoroughly ground with KBr. The Globar was used as an IR radiation source, and it was equipped with a KBr wide range beamsplitter and RT-DLaTGS as a detector. The reflection spectra were recorded with the use of a Shimadzu UV-3600 spectrophotometer.

3. Results and discussion

3.1. X-ray diffraction and crystal structure

In the Rietveld structure refinement, the structure of $BaNdCuS_3$ was used as a starting model and the Nd ion site was assumed as that occupied by Dy, Ho or Yb ions (Fig. 2) according to the suggested chemical formula $BaLnCuS_3$ (Ln = Dy, Ho, Yb). The refinements were stable and gave low *R*-factors, as shown in Fig. 3 and Table 1. The atom coordinates and main bond lengths are given in Tables 2 and 3, respectively. The linear dependence of cell volume *V* on the *IR* radii of the Ln ion in $BaLnCuS_3$ (Ln = Dy, Ho, Yb) proves the close similarity of the suggested and real chemical compositions (Fig. 3d). The crystallographic data are deposited in Cambridge Crystallographic Data Centre (CCDC # 2048615–2048617). The data can be downloaded from the site (www.ccdc.cam.ac.uk/data_request/cif).

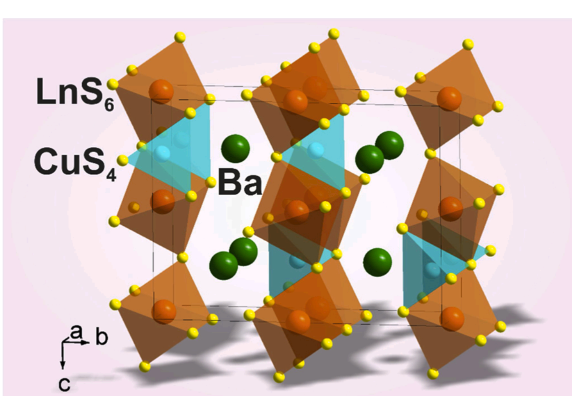

Fig. 2. Crystal structure of $BaLnCuS_3$ (Ln = Dy, Ho, Yb). The unit cell is outlined. The lone atoms, except barium, are omitted for clarity.

As it is known, the compounds $ABCX_3$ (A = Sr, Ba, Eu^{2+}, Pb^{2+}; B = Ln, Y; C = Cu; X = S, Se) crystallized in *Cmcm* or *Pnma* structures. Previously, the tolerance factor $t = IR(A)\times IR(C)/IR(B)^2$ was introduced and it controls the appearance of *Cmcm* or *Pnma* structures depending on the selection of A, B and C elements in $ABCX_3$ compounds [46]. According to the analysis carried out in [46], the *Cmcm* structure was predicted for the compounds $ABCX_3$ with $t > 0.908$. The tolerance factors calculated for sulfides $BaLnCuS_3$ (Ln = Dy, Ho, Yb) are given in Table 4 and the related points are presented in the diagram shown in Fig. 4. The ion radii values reported in [52] were used in the calculations. As it is seen, the compounds $BaLnCuS_3$ (Ln = Dy, Ho, Yb) should crystallize in space group *Cmcm*, and this prediction is successfully confirmed in the experiment implemented in the present study. This result confirms that the tolerance factor *t* well controls the formation of *Cmcm* or *Pnma* structures in the compounds $ABCuX_3$ (A = Sr, Ba, Eu^{2+}, Pb^{2+}; B = Ln, Y; X = S, Se).

3.2. Morphology

The microstructure of $BaLnCuS_3$ (Ln = Dy, Ho, Yb) samples prepared by sulfidation method is shown in Fig. 5 and 1S. In general, the particle morphologies of all three samples are similar. According to the SEM observation, the obtained sulfide products are mostly formed by spongy agglomerates of 10−100 μm in size. The agglomerates contain partly coalesced 1−5 μm grains. The contrast in SEM patterns is uniform and it confirms the chemical composition homogeneity.

3.3. Thermal properties

In the DSC/TG experiments, the samples of $BaDyCuS_3$ and $BaHoCuS_3$ were brought to the melting state two times. However, one heating/cooling cycle was recorded for $BaYbCuS_3$. First, the $BaDyCuS_3$ and $BaHoCuS_3$ samples were heated up to the melting state and, in this heating/cooling cycle, the number of heat effects, possible weight loss and melting temperature were estimated. Besides, after the cooling and solidification, the sample is in a tight contact to the crucible walls and this is a significant factor for the precise measurement of thermal parameters. Thus, the first heating was carried out from 10 to 1600 °C. Only one heating/cooling cycle from 10 to 1450 °C was implemented for $BaYbCuS_3$. No weight loss was recorded for all compounds and it indicated their high thermal stability. The second heating to 1450 °C was carried out for the measurements and the resulted curves are shown in Fig. 6. The obtained melting temperatures and heats of melting are listed in Table 5. As shown in Fig. 6, the melting point is determined by the extrapolation from the maximum melting point at the tangential point of the melting start to the heating baseline [53]. This method is applied because of the wide melting range and the presence of thermal gradient in the sample.

In all three substances, only one melting effect was observed, and no other thermal effects were detected on heating. $BaDyCuS_3$ and $BaHoCuS_3$ melt congruently at 1376 and 1363 °C, respectively. $BaYbCuS_3$ melts incongruently at the temperature of 1353 °C. In $BaYbCuS_3$, two superimposed crystallization peaks were clearly registered upon cooling and this is a robust indicator of the compound decomposition on melting. As it is seen in Table 5, at the transition from Dy to Ho and Yb, the melting temperature decreases by 23 °C. The enthalpy of fusion, in turn, increases by nearly twice and it reaches the level as high as 162.8 ± 4.8 kJ/mol in $BaYbCuS_3$.

Then, it is intriguing to compare the thermal parameters determined for $BaLnCuS_3$ (Ln = Dy, Ho, Yb) samples with those previously reported for other sulfides $ALnCuS_3$ (A = Sr, Ba, Eu^{2+}). The values of temperature and entalpy of melting in the known sulfides $ALnCuS_3$ (A = Sr, Ba, Eu^{2+}) are summarized in Tables 1S and 2S, respectively, and the related experimental points are displayed in Fig. 7 [24,26,34,46,47,54,55]. As

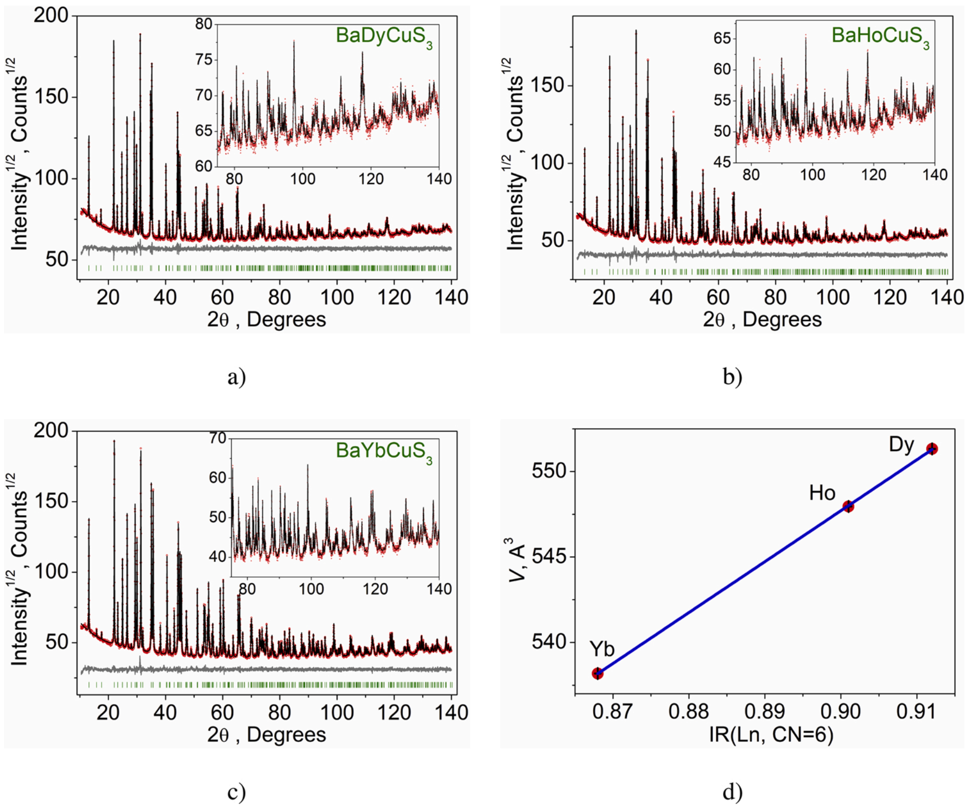

Fig. 3. Difference Rietveld plots of $BaLnCuS_3$: (a) Ln = Dy; (b) Ln = Ho; (c) Ln = Yb. Linear cell volume dependence *V*(*IR*) per ion radii *IR* (d).

Table 1
Main parameters of processing and refinement of the $BaLnCuS_3$ (Ln = Dy, Ho, Yb) samples.

Ln	Space group	Cell parameters (Å), Cell Volume (Å^3)	R_{wp}, R_p, R_B, χ^2
Dy	*Cmcm*	*a* = 4.02150 (3), *b* = 13.4455 (1), *c* = 10.19622 (8), *V* = 551.319 (7)	2.13, 1.62, 1.23, 1.47
Ho	*Cmcm*	*a* = 4.01228 (3), *b* = 13.4364 (1), *c* = 10.16414 (8), *V* = 547.955 (8)	2.80, 2.12, 1.51, 1.56
Yb	*Cmcm*	*a* = 3.98469 (2), *b* = 13.42090 (7), *c* = 10.06351 (5), *V* = 538.178 (5)	3.11, 2.31, 0.79, 1.53

Table 2
Fractional atom coordinates and isotropic displacement parameters (Å^2) of $BaLnCuS_3$ (Ln = Dy, Ho, Yb).

Atom	*x*	*y*	*z*	B_{iso}	Occupancy
Ln = Dy					
Dy	0.5	0	0	0.24 (3)	1
Cu	0.5	0.53360 (16)	0.25	0.39 (6)	1
Ba	0.5	0.25577 (7)	0.25	0.35 (3)	1
S1	0.5	0.63402 (19)	0.0613 (2)	0.50 (7)	1
S2	0.5	0.9321 (3)	0.25	0.56 (9)	1
Ln = Ho					
Ho	0.5	0	0	0.16 (3)	1
Cu	0.5	0.53282 (14)	0.25	0.46 (5)	1
Ba	0.5	0.25608 (7)	0.25	0.42 (3)	1
S1	0.5	0.63344 (17)	0.0599 (2)	0.50 (6)	1
S2	0.5	0.9346 (2)	0.25	0.56 (8)	1
Ln = Yb					
Yb	0.5	0	0	0.43 (4)	1
Cu	0.5	0.53355 (11)	0.25	0.85 (5)	1
Ba	0.5	0.25536 (6)	0.25	0.65 (4)	1
S1	0.5	0.63083 (16)	0.05789 (18)	0.50 (6)	1
S2	0.5	0.9343 (2)	0.25	0.56 (8)	1

to the melting temperature variation, as shown in Fig. 7a, the general trends are similar in $ALnCuS_3$ (A = Sr, Eu^{2+}). First, on the move from La to Nd, the T_m value decreases to the minimum at 1429 and 1470 °C in $SrNdCuS_3$ and $EuNdCuS_3$, respectively. However, on the further move from Nd to Er, the drastic increase of T_m is evident up to the record level of 1720−1735 °C in $EuLnCuS_3$ (Ln = Gd, Dy, Er). It should be mentioned that the position of minimum on this noncontinuous curve is less clear because the thermal parameters of sulfides $APmCuS_3$ (A = Sr, Eu^{2+}) remain unknown. With a high probability, the compounds $APmCuS_3$ (A = Sr, Eu^{2+}) can just have the minimum T_m values. Comparatively, other trend is observed in sulfides $BaLnCuS_3$. In these crystals, a continuous increase of T_m is observed on the move from La to Yb. Generally, it can be concluded that, in compounds $ALnCuS_3$ (A = Sr, Ba, Eu^{2+}), the high melting temperatures are characteristic of the sulfides of heavy Ln elements.

The variation of enthalpy of melting in compounds $ALnCuS_3$ (A = Sr, Ba, Eu^{2+}) is shown in Fig. 7b. The values of H_m are relatively low in $ALnCuS_3$ (A = Sr, Eu^{2+}; Ln = La, Ce, Pr, Nd) and $BaLaCuS_3$, and the extremely low values of H_m are observed in $SrSmCuS_3$ and $EuLnCuS_3$ (Ln = Sm, Gd, Dy, Er). Contrary to that, a drastic increase in H_m is observed in $BaLnCuS_3$ (Ln = Pr, Dy, Ho, Yb). On this basis, even a higher H_m value could be assumed in $BaLuCuS_3$ if this sulfide exists. As for now, a satisfactory explanation of so specific behavior of thermal parameters for compounds $BaLnCuS_3$ is elusive and a further accumulation of experimental results is topical.

3.4. Optical properties

The investigation of the optical properties of sulfides is of great importance to define their possible applications in photonics. As an example, the optimal bandgap of semiconductors for photovoltaic

Table 3
Main bond lengths (Å) in $BaLnCuS_3$ (Ln = Dy, Ho, Yb).

Ln = Dy			
Dy—S1[i]	2.7713 (18)	Cu—S1	2.351 (3)
Dy—S2[ii]	2.7074 (11)	Cu—S2[iii]	2.430 (2)
Ln = Ho			
Ho—S1[i]	2.7585 (16)	Cu—S1	2.359 (2)
Ho—S2[ii]	2.6889 (10)	Cu—S2[iii]	2.4016 (19)
Ln = Yb			
Yb—S1[i]	2.7188 (14)	Cu—S1	2.333 (2)
Yb—S2[ii]	2.6660 (9)	Cu—S2[iii]	2.3967 (17)

Symmetry codes: (i) -*x*+1/2, -*y*+1/2, -*z*; (ii) *x*, *y*-1, *z*; (iii) -*x*+1/2, *y*-1/2, -*z*+1/2.

Table 4
Calculated tolerance factors *t* and predicted space group of compounds $BaLnCuS_3$ (Ln = Dy, Ho, Yb).

Compound	*t*	Space group	Reference
$BaDyCuS_3$	1.024	*Cmcm*	This study
$BaHoCuS_3$	1.050	*Cmcm*	This study
$BaYbCuS_3$	1.131	*Cmcm*	This study

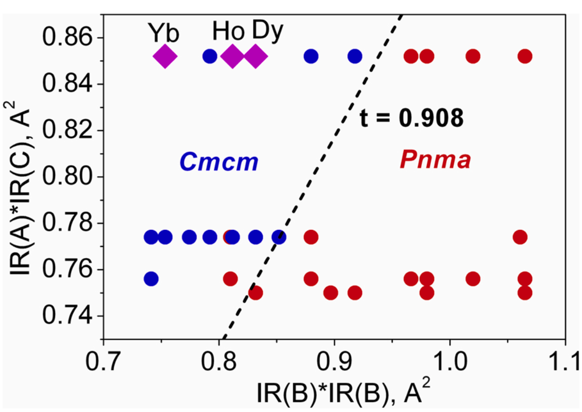

Fig. 4. Structure types in the known $ABCX_3$ (X = S, Se) crystals. The compounds $BaDyCuS_3$, $BaHoCuS_3$ and $BaYbCuS_3$ are shown in magenda color.

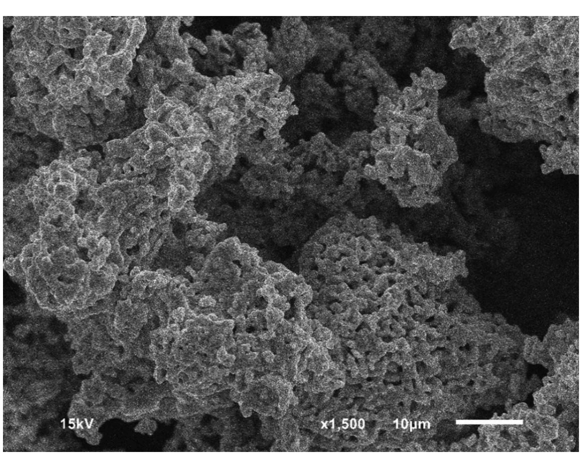

Fig. 5. SEM pattern of the $BaDyCuS_3$ sample prepared by the sulfidation reaction.

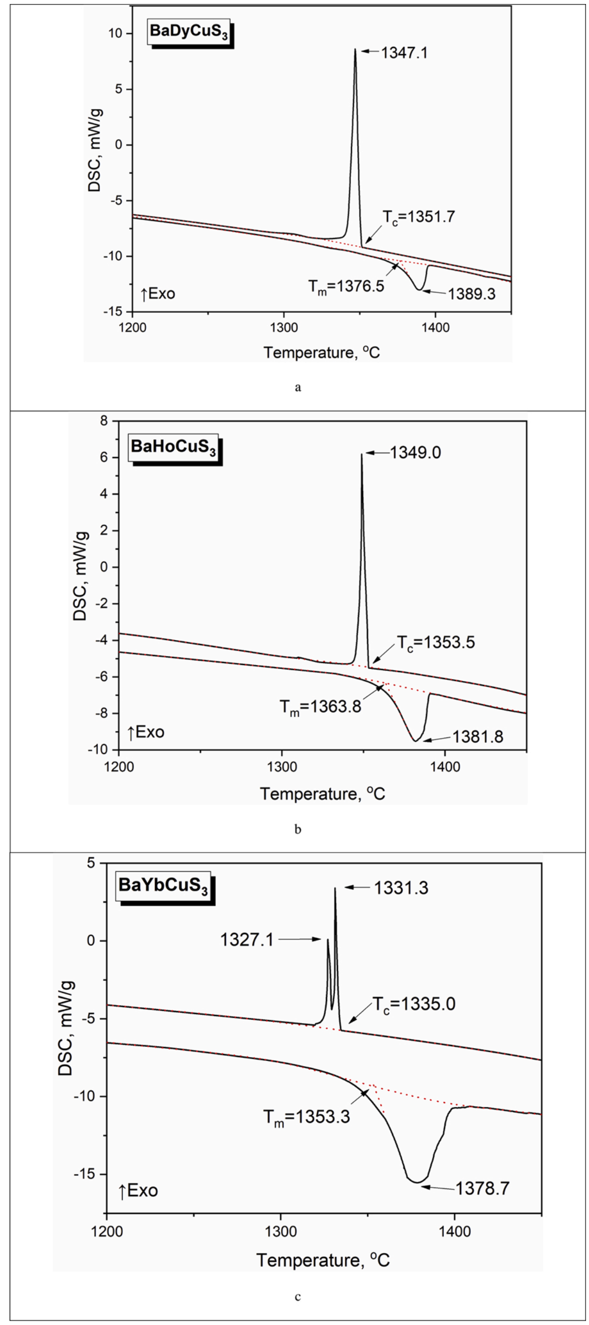

Fig. 6. DTA curves recorded for (a) BaDyCuS3, (b) $BaHoCuS_3$ and (c) $BaYbCuS_3$. The baselines are shown in red color (For interpretation of the references to colour in this figure legend, the reader is referred to the web version of this article).

Table 5
Melting temperatures and enthalpies of compounds synthesized in this contribution.

Compound	Melting point, °C	Enthalpy of fusion, kJ/mol
$BaDyCuS_3$	1376 ± 2	91.4 ± 2.7
$BaHoCuS_3$	1363 ± 2	125.9 ± 3.8
$BaYbCuS_3$	1353 ± 2	162.8 ± 4.8

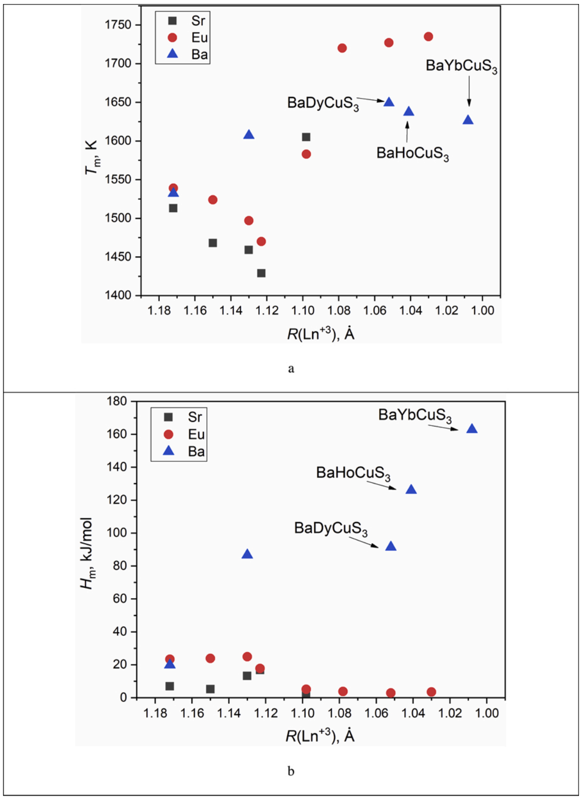

Fig. 7. Dependences of (a) melting temperature and (b) enthalpy of melting on the effective ion radii of the Ln element in compounds $ABCuS_3$ (A = Sr, Ba, Eu^{2+}; B = Ln).

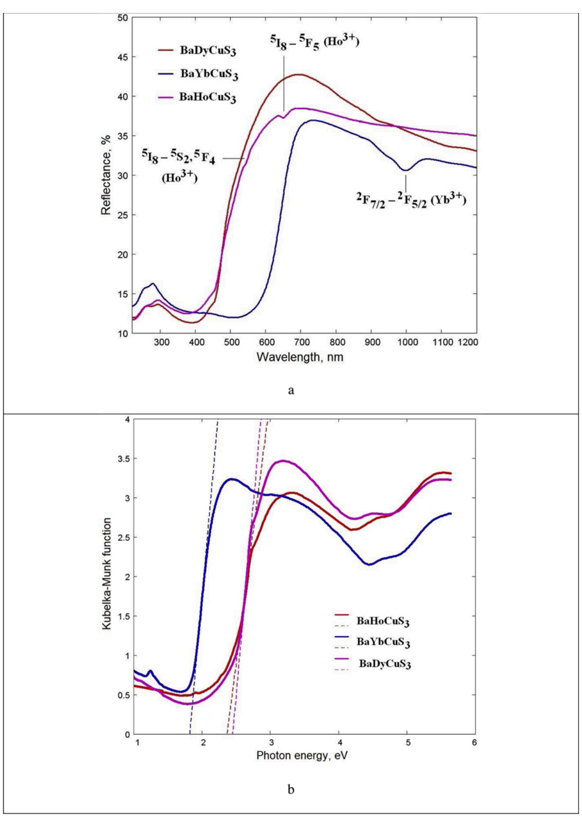

Fig. 8. Reflection spectra of $BaDyCuS_3$, $BaHoCuS_3$ and $BaYbCuS_3$ and related Kubelka-Munk plots.

structures is 1.4–1.5 eV [56,57]. In such advanced photovoltaic chalcogenide as CIGS, the bandgap can be tuned in the range of 1.0-1.7 eV by the chemical composition variation. The reflection spectra of $BaDyCuS_3$, $BaHoCuS_3$ and $BaYbCuS_3$ are presented in Fig. 8. In all three sulfides, the band edges are in the visible range. As is seen in Fig. 8a, the individual characteristic bands corresponding to the *f-f* transitions of rare earth ions are detected in $BaHoCuS_3$ and $BaYbCuS_3$. The band related to the $^2F_{7/2} - {}^2F_{5/2}$ transitions of Yb^{3+} ions is positioned in the region below 1000 nm for $BaYbCuS_3$, and, in the reflection spectrum of $BaHoCuS_3$, the well-pronounced $^5I_8 - {}^5F_5$ band at 660 nm and weakly pronounced $^5I_8 - {}^5S_2$, $^5F_4$ band at 550 nm can be observed. The Kubelka-Munk plots for $BaDyCuS_3$, $BaHoCuS_3$ and $BaYbCuS_3$ are presented in Fig. 8b. The optical bandgap values derived from Kubelka-Munk plotting are 2.45 eV for $BaDyCuS_3$, 2.37 eV for $BaHoCuS_3$ and 1.82 eV for $BaYbCuS_3$. While the bandgap values of $BaDyCuS_3$ and $BaHoCuS_3$ are typical of multication sulfide materials comprising a monovalent copper ion, alkaline-earth ion and one rare earth ion, the $BaYbCuS_3$ bandgap is noticeably smaller. Surprising is that the $BaYbCuS_3$ bandgap is even smaller than that in recently studied $EuErCuS_3$ (1.94 eV) [24], where the bandgap narrowing can be assigned to the 5d states of Eu^{2+} ion positioned at the conduction band bottom. As a possible explanation of the significant bandgap narrowing in $BaYbCuS_3$ with respect to isostructural $BaHoCuS_3$ and $BaDyCuS_3$, the presence of minor Yb^{2+} ion fraction in the crystal lattice (or, in a more complex case, the mixed valence state Yb^{2+}+Cu^{2+}) can be considered. To check this suggestion, we examined the $BaYbCuS_3$ luminescence under the excitation at 647 nm and at 410 nm. The characteristic luminescence of Yb^{2+} ions in sulfides in the near IR range was not detected. Therefore, the most probable explanation for the additional absorption of $BaYbCuS_3$ in the range of 500−600 nm and the corresponding bandgap narrowing must be explained by the charge transfer states associated with Yb^{3+}. Typically, these states in trivalent rare earth ions in oxides are at 5–6 eV. However, the divalent Yb ion with its electronic configuration f^{14} must have its enhanced stability of the completely filled *f* shell. This enhanced stability must lead to lower-lying charge-transfer states. Alongside with the lower electronegativity of sulfur, with respect to oxygen, the assignment of the bottom states of conduction band in $BaYbCuS_3$ as charge transfer states is reliable. This result shows that the optical bandgap of chalcogenides can be efficiently tuned by the addition of Yb^{3+}. However, the photovoltaic efficiency of charge transfer absorption needs an additional study.

3.5. *Vibrational spectroscopy*

The Raman and Infrared spectra of Ba*Ln*CuS_3 (*Ln* = Dy, Ho, Yb) are displayed in Fig. 9a and b, respectively. The Raman spectra of $BaDyCuS_3$ and $BaYbCuS_3$ shown in Fig. 9a were recorded under the excitation at 647.1 nm, whereas, to avoid excitation of the Ho^{3+} luminescence, the 1064 nm excitation wavelength was used in $BaHoCuS_3$. In the later case, the recording of spectral signal is possible only from 100 cm^{-1} [58].

The *Cmcm* crystal structure of investigated compounds contains two formula units ($Z = 2$) per primitive cell. The irreducible representations for vibrational modes associated with Ba, *Ln*, Cu and S atoms are listed in Table 6 [59]. Taking into account data from Table 6, the mechanical representation for Ba*Ln*CuS_3 (space group *Cmcm*) at the Brillouin zone center can be written as: $\Gamma_{vibr} = 5A_g + 2A_u + 4B_{1g} + 7B_{1u} + B_{2g} + 7B_{2u} + 5B_{3g} + 5B_{3u}$. The A_u modes are silent and $B_{1u} + B_{2u} + B_{3u}$ modes are acoustical. Herein, the *g*-labeled phonon modes are Raman active, while Infrared active modes are *u*-labeled.

As it was shown above, the tolerance factor *t* can be a useful indicator for the determination of $ABCX_3$ crystal structure symmetry [46]. In case of $BaLnCuS_3$ (Ln = Dy, Ho, Yb), this method showed that compounds under investigation should belong to *Cmcm* space group but not to *Pnma*, and this result is in agreement with the XRD data. As for the vibrational spectroscopy method, the Raman and Infrared spectra are strongly dependent on the arrangement of crystal structure units, and the number

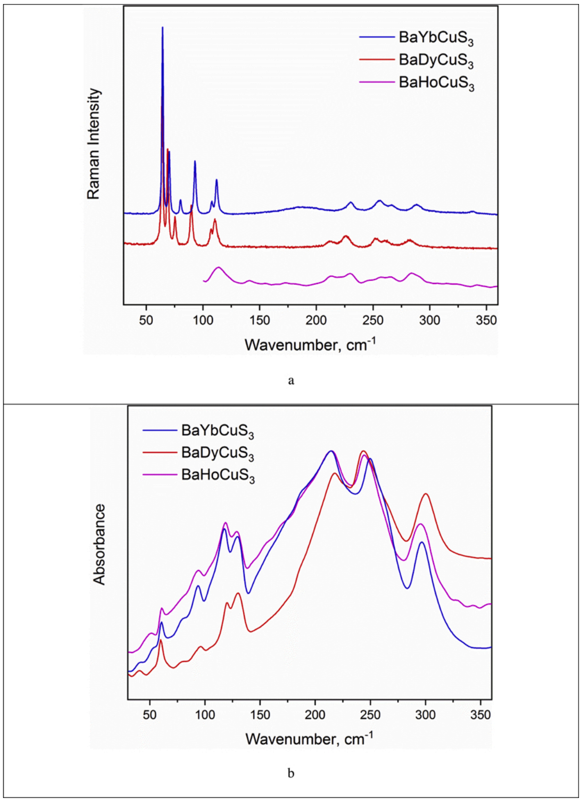

Fig. 9. (a) Raman spectra from $BaDyCuS_3$ and $BaYbCuS_3$ recorded with the excitation at 647.1 nm and the Raman spectrum of $BaHoCuS_3$ recorded with the excitation at 1064 nm, and (b) Infrared spectra of $BaLnCuS_3$ (Ln = Dy, Ho, Yb) in the Far-IR subregion.

Table 6
The irreducible representations for Raman and Infrared modes in Ba*Ln*CuS_3 (*Ln* = Dy, Ho, Yb) in respect to the positions of atoms.

Atom	Wyckoff position	Irreducible representations
Ln	4*b*	$2B_{1u} + 2B_{2u} + B_{3u}$
Cu, Ba, S2	4*c*	$A_g + B_{1g} + B_{3g} + B_{1u} + B_{2u} + B_{3u}$
S1	8*f*	$2A_g + B_{1g} + B_{2g} + 2B_{3g} + 2B_{1u} + 2B_{2u} + B_{3u}$

and activity of vibrations in spectra are determined by the crystal symmetry [60]. However, it is hard to find the difference between experimental Raman spectra of Ba*Ln*CuS_3 compounds crystallized in space groups *Cmcm* and *Pnma* in the case of powder samples because the polarized spectra can not be recorded [46]. As it can be seen in Fig. 9a and b, the Raman and Infrared spectral profiles of $BaHoCuS_3$, $BaDyCuS_3$ and $BaYbCuS_3$ are almost identical with a small shift in wavenumber values and it verifies that these compounds are isostructural. The positions of spectral bands of all compounds under investigation are presented in Table 3S. On the other hand, it can be clearly seen that the Infrared spectra of *Cmcm* and *Pnma* members of the Ba*Ln*CuS_3 family are noticeably different, as exhibited in Fig. 2S [26]. This fact confirms that Ba*Ln*CuS_3 (*Ln* = Dy, Ho, Yb) compounds are isostructural and belong to the *Cmcm* space group, but not to that of *Pnma*. As it can be observed in Fig. 9a and b, the vibrational modes of Ba*Ln*CuS_3 (*Ln* = Dy, Ho, Yb) are located in the range of 50–350 cm^{-1}, and that is in agreement with the vibrational spectra of other orthorhombic (space group *Cmcm*) Ba*Ln*CuS_3 crystals [46]. As it was previously shown [46], the vibrational modes below 150 cm^{-1} are associated with the vibrations of the layers formed with CuS_4 tetrahedra and *Ln*S_6 octahedra which form crystal structure of Ba*Ln*CuS_3 compounds. The spectral region between 190 and 290 cm^{-1} contains bands related to the vibrations of predominantly sulfur ions, while the spectral bands above 290 cm^{-1} are attributed to the stretching-like modes of tetrahedral CuS_4 groups.

4. Conclusions

This study addresses the synthesis, structure, optical and thermal properties of the new complex sulfides $BaDyCuS_3$, $BaHoCuS_3$ and $BaYbCuS_3$. All three compounds crystallize in the *Cmcm* space group ($KZrCuS_3$ structural type). According to structural and vibrational properties, all substances are in the single phase state. The compounds have a linear change in unit cell parameters, as induced by the substitution of Ln element. Also, the symmetry of the phases is consistent with the tolerance factor introduced earlier for this crystal family. The powder samples morphology is described by the irregular agglomerates consisting of particles ranging in size from 1 to 5 μm. $BaDyCuS_3$ and $BaHoCuS_3$ melt congruently at 1376.5 and 1363.8 °C, respectively. However, $BaYbCuS_3$ melts incongruently at 1353.3 °C. The compounds are characterized by extremely high enthalpy of fusion in the range of 91.4–162.8 kJ/mol, and the value obtained for $BaYbCuS_3$ (162.8 kJ/mol) is the highest known in $ABCuX_3$ (A = Sr, Ba, Eu^{2+}, Pb^{2+}; B = Ln, Y). The optical band gap is 2.45 eV for $BaDyCuS_3$, 2.37 eV for $BaHoCuS_3$ and 1.82 eV for $BaYbCuS_3$. The anomalous decrease of the bandgap for $BaYbCuS_3$ is explained by the charge transfer band of Yb at the bottom of conduction band. This finding can be of importance in photovoltaics for tuning the bandgap of complex sulfides by the addition of Yb^{3+} ions.

Author statement

Nikita O. Azarapin Conceptualization; Data curation; Roles/Writing - original draft
Victor V. Atuchin Conceptualization; Writing - review & editing
Nikolai G. Maximov Data curation
Aleksandr S. Aleksandrovsky Data curation; Roles/Writing - original draft
Maxim S. Molokeev Data curation; Formal analysis; Roles/Writing - original draft
Aleksandr S. Oreshonkov Formal analysis; Roles/Writing - original draft
Nikolai P. Shestakov Data curation
Alexander S. Krylov Data curation
Tatyana M. Burkhanova Methodology
Shaibal Mukherjee Methodology; Writing - review & editing
Oleg V. Andreev Conceptualization; Supervision

Declaration of Competing Interest

The authors declare that they have no known competing financial interests or personal relationships that could have appeared to influence the work reported in this paper.

Acknowledgements

This study was supported by the Russian Science Foundation (19-42-02003). The authors would like to thank Alexey A. Lubin for his studies on SEM. The studies were carried out on the basis of laboratory of electron and probe microscopy in REC ‘Nanotechnologies’. This work was partially supported by the DST-RSF project under the India-Russia Programme of Cooperation in Science and Technology (No. DST/ INT/ RUS/RSF/P-20 dated May 16, 2019). Shaibal Mukherjee would like to thank MeitY for the YFRF under the Visvesvaraya Ph.D. Scheme for Electronics and IT. This publication is an outcome of the R&D work undertaken in the project under the Visvesvaraya Ph.D. Scheme of MeitY being implemented by Digital India Corporation (formerly Media Lab Asia). We are grateful to the Krasnoyarsk Regional Center of Research Equipment of the Federal Research Center « Krasnoyarsk Science Center SB RAS » for the provided equipment.

Appendix A. Supplementary data

Supplementary material related to this article can be found, in the online version, at doi:https://doi.org/10.1016/j.materresbull.2021.111314.

References

[1] L.A. Koscielski, J.A. Ibers, The structural chemistry of quaternary chalcogenides of the type AMM'Q$_3$, Z. Anorg. Allg. Chem. 638 (15) (2012) 2585–2593.
[2] M. Frumar, T. Wagner, K. Shimakawa, B. Frumarova, Crystalline and amorphous chalcogenides, high-tech materials with structural disorder and many important applications, NATO Sci. Peace Secur. Series C: Environ. Secur. 139 (2015) 151–238.
[3] Zhi-Shu Feng, Zhi-Hui Kang, Feng-Guang Wu, Jin-Yue Gao, Yun Jiang, Hong-Zhi Zhang, Yury M. Andreev, Grigory V. Lanskii, Viktor V. Atuchin, Tatyana A. Gavrilova, SHG in doped GaSe: in crystals, Opt. Express 16 (13) (2008) 9978–9985.
[4] V.V. Atuchin, V.A. Golyashov, K.A. Kokh, I.V. Korolkov, A.S. Kozhukhov, V. N. Kruchinin, S.V. Makarenko, L.D. Pokrovsky, I.P. Prosvirin, K.N. Romanyuk, O. E. Tereshchenko, Formation of inert Bi_2Se_3(0001) cleaved surface, Cryst. Growth Des. 11 (2011) 5507–5514.
[5] Wenlong Yin, Kai Feng, Ran He, Dajiang Mei, Zheshuai Lin, Jiyong Yao, Yicheng Wu, $BaGa_2MQ_6$ (M = Si, Ge; Q = S, Se): a new series of promising IR nonlinear optical materials, Dalton Trans. 41 (2012) 5653–5661.
[6] Vishnu Awasthi, Sushil K. Pandey, Saurabh K. Pandey, Shruti Verma, Mukul Gupta, Shaibal Mukherjee, Growth and characterizations of dual ion beam sputtered CIGS thin films for photovoltaic applications, J. Mater. Sci. : Mater. Electron. 25 (2014) 3069–3076.
[7] S.A. Bereznaya, Z.V. Korotchenko, R.A. Redkin, S.Yu. Sarkisov, V.N. Brudnyi, A. V. Kosobutsky, V.V. Atuchin, Terahertz generation from electron- and neutron-irradiated semiconductor crystal surfaces, Infrared Phys. Technol. 77 (2016) 100–103.
[8] Brajendra S. Sengar, Vivek Garg, Vishnu Awasthi, Shailendra Kumar Aaryashree, C. Mukherjee, Mukul Gupta, Shaibal Mukherjee, Growth and characterization of dual ion beam sputtered $Cu_2ZnSn(S,Se)_4$ thin films for cost-effective photovoltaic application, Sol. Energy 139 (2016) 1–12.
[9] Brajendra S. Sengar, Vivek Garg, Amitesh Kumar, Vishnu Awasthi, Shailendra Kumar, Victor V. Atuchin, Shaibal Mukherjee, Band alignment of Cd-free (Zn, Mg)O layer with $Cu_2ZnSn(S,Se)_4$ and its effect on the photovoltaic properties, Opt. Mater. 84 (2018) 748–756.
[10] Yankun Wen, Han Zhu, Lingling Zhang, Songge Zhang, Ming Zhang, Mingliang Du, Activating MoS_2 by interface engineering for efficient hydrogen evolution catalysis, Mater. Res. Bull. 112 (2019) 46–52.
[11] S. Cheng, X. Zhang, M. Lee, J. Zhang, Hierarchy in nonlinear optical responses induced by metal cation tailoring effect in the In-containing chalcogenide compounds, J. Alloys Compd. 788 (2019) 1021–1028.
[12] Yuriy G. Denisenko, Maxim S. Molokeev, Alexander S. Krylov, Aleksandr S. Aleksandrovsky, AleksandrS. Oreshonkov, Victor V. Atuchin, Nikita O. Azarapin, Pavel E. Plyusnin, Elena I. Sal'nikova, Oleg V. Andreev, High-temperature oxidation of europium (II) sulfide, J. Indust. Eng. Chem. 79 (2019) 62–70.
[13] Yixuan Shi, Cheryl Sturm, Holger Kleinke, Chalcogenides as thermoelectric materials, J. Solid State Chem. 270 (2019) 273–279.
[14] Hyun-Jun Hwang, Cheng Zeng, Changqing Pan, Michael Dexter, Rajiv Malhotra, Chih-hung Chang, Tuning electronic and photocatalytic properties in pulsed light synthesis of Cu_2ZnSnS_4 films from CuS-ZnS-SnS nanoparticles, Mater. Res. Bull. 122 (2020), 110645.
[15] J. Gospodarič, V. Dziom, A. Shuvaev, A.A. Dobretsova, N.N. Mikhailov, Z.D. Kvon, E.G. Novik, A. Pimenov, Band structure of a HgTe-based three-dimensional topological insulator, Phys. Rev. B 102 (2020), 115113.
[16] Aleksandr V. Sotnikov, Vladimir V. Bakovets, Evgeniy V. Korotaev, Svetlana V. Trubina, Vladimir I. Zaikovskii, Short- and long-range disorders in misfit layered compounds $(MS)_{1.2+q}NbS_2$ with the solid solution subsystem (MS) = $(Gd_xDy_{1-x}S)$, Mater. Res. Bull. 131 (2020), 110963.
[17] Patrick Gougeon, Philippe Gall, Shantanu Misra, Anne Dauscher, Christophe Candolfi, Bertrand Lenoir, Synthesis, crystal structure and transport properties of the cluster compounds $Tl_2Mo_{15}S_{19}$ and $Ag_3Tl_2Mo_{15}S_{19}$, Mater. Res. Bull. 136 (2021), 111152.
[18] Ping Wu, Amy E. Christuk, James A. Ibers, New quaternary chalcogenides $BaLnMQ_3$ (Ln = rare earth or Sc; M = Cu, Ag; Q = S, Se). II. Structure and property variation vs rare-earth element, J. Solid State Chem. 110 (1994) 337–344.
[19] V.P. Sachanyuk, G.P. Gorgut, V.V. Atuchin, I.D. Olekseyuk, O.V. Parasyuk, The Ag_2S-In_2S_3-$Si(Ge)S_2$ systems and crystal structure of quaternary sulfides $Ag_2In_2Si(Ge)S_6$, J. Alloys Compd. 452 (2008) 348–358.
[20] Ali H. Reshak, V.V. Atuchin, S. Auluck, I.V. Kityk, First and second harmonic generation of optical susceptibilities for the non-centro-symmetric orthorhombic $AgCd_2GaS_4$, J. Phys. Condens. Matter 20 (2008), 325234.
[21] Dajiang Mei, Shiyan Zhang, Fei Liang, Sangen Zhao, Jianqiao Jiang, Junbo Zhong, Zheshuai Lin, Wu Yuandong, $LiGaGe_2S_6$: a chalcogenide with good infrared nonlinear optical performance and low melting point, Inorg. Chem. 56 (21) (2017) 13267–13273.
[22] A.A. Ionin, D.V. Badikov, V.V. Badikov, I.O. Kinyaevskiy, Yu.M. Klimachev, A. A. Kotkov, A.Yu. Kozlov, A.M. Sagitova, D.V. Sinitsyn, Sum frequency generation of multi-line slab radio frequency discharge carbon monoxide laser system with intracavity nonlinear $BaGa_2GeSe_6$ crystal, Opt. Lett. 43 (18) (2018) 4358–4361.
[23] A.O. Fedorchuk, O.V. Parasyuk, O. Cherniushok, B. Andriyevsky, G.L. Myronchuk, O.Y. Khyzhun, G. Lakshminarayana, J. Jedryka, I.V. Kityk, A.M. ElNaggar, A. A. Albassam, M. Piasecki, $PbGa_2GeS_6$ crystal as a novel nonlinear optical material: band structure aspects, J. Alloys Compd. 740 (2018) 294–304.
[24] Anna V. Ruseikina, Leonid A. Solovyov, VladimirA. Chernyshev, Aleksandr S. Aleksandrovsky, Oleg V. Andreev, Svetlana N. Krylova, Alexander S. Krylov, DmitriyA. Velikanov, Maxim S. Molokeev, Nikolai G. Maximov, Maxim V. Grigoriev, Alexander A. Garmonov, Alexey V. Matigorov, Synthesis, structure, and properties of $EuErCuS_3$, J. Alloys Compd. 805 (2019) 779–788.
[25] Weikang Wang, Dajiang Mei, Fei Liang, Jun Zhao, Yuandong Wu, Zheshuai Lin, Inherent laws between tetrahedral arrangement pattern and optical performance in tetrahedron-based mid-infrared nonlinear optical materials, Coord. Chem. Rev. 421 (2020), 213444.
[26] A.S. Oreshonkov, N.O. Azarapin, N.P. Shestakov, S.V. Adichtchev, Experimental and DFT study of $BaLaCuS_3$: direct band gap semiconductor, J. Phys. Chem. Solids 148 (2021), 109670.
[27] Amy E. Christuk, Ping Wu, James A. Ibers, New quaternary chalcogenides $BaLnMQ_3$ (Ln = rare earth; M= Cu, Ag; Q = S, Se. I. Structures and grinding-induced phase transition in $BaLaCuQ_3$, J. Solid State Chem. 110 (1994) 330–336.
[28] Yuting Yang, James A. Ibers, Synthesis and characterization of a series of quaternary chalcogenides $BaLnMQ_3$ (Ln = rare earth, M = coinage metal, Q = Se or Te), J. Solid State Chem. 147 (1999) 366–371.
[29] Fu Qiang Huang, Kwasi Mitchell, James A. Ibers, New layered materials: syntheses, structures, and optical and magnetic properties of $CsGdZnSe_3$, $CsZrCuSe_3$, $CsUCuSe_3$, and $BaGdCuSe_3$, Inorg. Chem. 40 (2001) 5123–5126.
[30] Kwasi Mitchell, Fu Qiang Huang, Adam D. McFarland, Christy L. Haynes, Rebecca C. Somers, Richard P.Van Duyne, James A. Ibers, The $CsLnMSe_3$ semiconductors (ln = rare-earth element, Y; m = Zn, Cd, Hg), Inorg. Chem. 42 (2003) 4109–4116.
[31] N.V. Sikerina, A.V. Solov'eva, E.N. Toroshchin, O.V. Andreev, Phase equilibria in the BaS-Cu_2S- Gd_2S_3 system, Russ. J. Inorg. Chem. 52 (12) (2007) 1982–1986.
[32] N.V. Sikerina, O.V. Andreev, I.P. Leven, Interactions in the SrS-Cu_2S-Ln_2S_3 (Ln = Gd or Er) systems and phase-formation laws in the SrS-Cu_2S-Ln_2S_3 (Ln = La-Lu) systems, Russ, J. Inorg. Chem. 53 (3) (2008) 455–459.
[33] A.V. Ruseikina, L.A. Solov'ev, O.V. Andreev, Crystal structures and properties of $SrLnCuS_3$ (Ln = La, Pr) Russ, J. Inorg. Chem. 59 (3) (2014) 196–201.
[34] A.V. Ruseikina, O.V. Andreev, E.O. Galenko, S.I. Koltsov, Trends in thermodynamic parameters of phase transitions of lanthanide sulfides $SrLnCuS_3$ (Ln = La-Lu), J. Therm. Anal. Calorim. 128 (2) (2017) 993–999.
[35] Vivek Garg, Brajendra S. Sengar, Vishnu Awasthi, Amitesh Kumar, Rohit Singh, Shailendra Kumar, C. Mukherjee, V.V. Atuchin, Shaibal Mukherjee, Investigation of dual-ion beam sputter-instigated plasmon generation in TCOs: a case study of GZO, ACS Appl. Mater. Interfaces 10 (2018) 5464–5474.
[36] Vivek Garg, Brajendra S. Sengar, Amitesh Kumar, Gaurav Siddharth, Shailendra Kumar, Shaibal Mukherjee, Investigation of valence plasmon excitations in GMZO thin film and their suitability for plasmon-enhanced buffer-less solar cells, Sol. Energy 178 (2019) 114–124.
[37] Gaurav Siddharth, Vivek Garg, Brajendra S. Sengar, Ritesh Bhardwaj, Pawan Kumar, Shaibal Mukherjee, Analytical study of performance parameters of InGaN/GaN multiple quantum well solar cell, IEEE Trans. Elect. Devices 66 (8) (2019) 3399–3404.
[38] Gaurav Siddharth, Brajendra S. Sengar, Vivek Garg, Md Arif Khan, Ruchi Singh, Shaibal Mukherjee, Analytical performance analysis of CdZnO/ZnO-based multiple quantum well solar cell, IEEE Trans. Elect. Devices 67 (3) (2020) 1047–1051.
[39] Claudia Coughlan, Maria Ibáñez, Oleksandr Dobrozhan, Ajay Singh, Andreu Cabot, Kevin M. Ryan, Compound copper chalcogenide nanocrystals, Chem. Rev. 117 (2017) 5865–6109.
[40] Mai Nguyen, Kaia Ernits, Kong Fai Tai, Chin Fan Ng, Stevin Snellius Pramana, Wardhana A. Sasangka, Sudip K. Batabyal, Timo Holopainen, Dieter Meissner, Axel Neisser, Lydia H. Wong, ZnS buffer layer for $Cu_2ZnSn(SSe)_4$ monograin layer solar cell, Sol. Energy 111 (2015) 344–349.
[41] Kunpeng Zhao, Anders Bank Blichfeld, Espen Eikeland, Pengfei Qiu, Dudi Ren, Brummerstedt Iversen Bo, Xun Shi, Lidong Chen, Extremely low thermal conductivity and high thermoelectric performance in liquid-like $Cu_2Se_{1-x}S_x$ polymorph materials, J. Mater. Chem. A 5 (2017) 18148–18156.
[42] Tian-Ran Wei, Yuting Qin, Tingting Deng, Qingfeng Song, Binbin Jiang, Ruiheng Liu, Pengfei Qiu, Xun Shi, Lidong Chen, Copper chalcogenide thermoelectric materials, Sci. China Mater. 62 (1) (2019) 8–24.
[43] Sonam Maiti, Santanu Maiti, Ali Hossain Khan, Andreas Wolf, Dirk Dorfs, Iwan Moreels, Frank Schreiber, Marcus Scheele, Dye-sensitized ternary copper chalcogenide nanocrystals: optoelectronic properties, air stability, and photosensitivity, Chem. Mater. 31 (7) (2019) 2443–2449.
[44] P. Lemoine, D. Carre, M. Guittard, Structure du sulfured'europium et de cuivre Eu_2CuS_3, Acta Cryst. C 42 (1986) 390–391.
[45] Michael F. Mansuetto, Patricia M. Keane, James A. Ibers, Synthesis, structure, and conductivity of the new group IV chalcogenides $KCuZrQ_3$ (Q = S, Se, Te), J. Solid State Chem. 101 (1992) 257–264.
[46] N.O. Azarapin, A.S. Aleksandrovsky, V.V. Atuchin, T.A. Gavrilova, A.S. Krylov, M. S. Molokeev, S. Mukherjee, A.S. Oreshonkov, O.V. Andreev, Synthesis, structural and spectroscopic properties of orthorhombic compounds $BaLnCuS_3$ (Ln = Pr, Sm), J. Alloys Compd. 832 (2020), 153134.
[47] A.V. Ruseikina, O.V. Andreev, Phase equilibria in systems $DyCuS_2$-Eu-S and Cu_2S-Dy_2S_3-EuS, Russ. J. Inorg. Chem. 63 (11) (2018) 1494–1500.

[48] N.A. Khritohin, O.V. Andreev, O.V. Mitroshin, A.S. Korotkov, Thermodynamics of phase changes in systems BaS-Ln_2S_3 (Ln = Pr, Sm, Gd, Tb, Er, Lu, J. Phase Equilib. Diffusion 25 (6) (2004) 515–519.
[49] A.V. Ruseikina, O.V. Andreev, Phase equilibria in the Cu_2S-La_2S_3-EuS system, Russ. J. Inorg. Chem. 62 (5) (2017) 610–618.
[50] Bruker AXS TOPAS V4, General Profile and Structure Analysis Software for Powder Diffraction Data, – User's Manual, Bruker AXS, Karlsruhe, Germany, 2008.
[51] NETZSCH Proteus 6, Thermic Analyses – User's and Software Manuals, Germany, 2012.
[52] R.D. Shannon, Revised effective ionic radii and systematic studies of interatomic distances in halides and chalcogenides, Acta Cryst. A 32 (1976) 751–767.
[53] B. Wunderlich, Thermal Analysis, Academic Press, San Diego, California, 1990.
[54] Y.A. Murashko, A.V. Ruseikina, A.A. Kislitsyn, O.V. Andreev, Optical and thermal properties of the $EuLnCuS_3$ (Ln= La, Pr, Sm, Gd) compounds, Inorg. Mater. 51 (12) (2015) 1213–1218.
[55] A.V. Ruseikina, O.V. Andreev, Synthesis of compounds $EuLnCuS_3$ (Ln = La-Bd, their temperature and enthalpy of melting, Vestnik of Tyumen State University, Ecol. Nat. Manage. (3) (2010) 221–3227 (in Russian).
[56] Parag S. Vasekar, Anant H. Jahagirdar, Neelkanth G. Dhere, Photovoltaic characterization of Copper–Indium–Gallium Sulfide (CIGS2) solar cells for lower absorber thicknesses, Thin Solid Films 518 (7) (2010) 1788–1790.
[57] A.S. Oreshonkov, E.M. Roginskii, V.V. Atuchin, New candidate to reach Shockley-Queisser limit: the DFT study of orthorhombic silicon allotrope Si(oP32), J. Phys. Chem. Solids 137 (2020), 109219.
[58] A.S. Oreshonkov, N.P. Shestakov, M.S. Molokeev, A.S. Aleksandrovsky, I.A. Gudim, V.L. Temerov, S.V. Adichtchev, A.M. Pugachev, I.V. Nemtsev, E.I. Pogoreltsev, Y. G. Denisenko, Monoclinic $SmAl_3(BO_3)_4$: synthesis, structural and spectroscopic properties, Acta Crystallogr. B 76 (4) (2020) 654–660.
[59] E. Kroumova, M.I. Aroyo, J.M. Perez-Mato, A. Kirov, C. Capillas, S. Ivantchev, H. Wondraschek, Bilbao crystallographic server: useful databases and tools for phase-transition studies, Phase Transit. 76 (2003) 155–170.
[60] T.N. Moroz, N.A. Palchik, The uniqueness of determination of the space group symmetry by means of the vibrational spectroscopy methods, Crystallogr. Rep. 54 (5) (2009) 734–737.